Journal of Solid State Chemistry 184 (2011) 3208–3215

Contents lists available at SciVerse ScienceDirect

Journal of Solid State Chemistry

journal homepage: www.elsevier.com/locate/jssc

Evidence for transition from polaron to bipolaron conduction in electroactive $Li_xCr_{0.11}V_2O_{5.16}$ powders: A dynamic study from 10 to 10^{10} Hz

J.C. Badot [a,*], O. Dubrunfaut [b]

[a] Laboratoire de Chimie de la Matière Condensée de Paris, CNRS UMR 7574, ENSCP, Chimie ParisTech, 11 rue Pierre et Marie Curie, 75231 Paris Cedex 05, France
[b] Laboratoire de Génie Electrique de Paris, CNRS UMR 8507, SUPELEC, UPMC Univ Paris 06, Univ Paris-Sud, 11 rue Joliot-Curie, Plateau de Moulon, 91192 Gif-sur-Yvette Cedex, France

ARTICLE INFO

Article history:
Received 17 June 2011
Received in revised form
26 September 2011
Accepted 3 October 2011
Available online 12 October 2011

Keywords:
Dielectric relaxation
Electronic conduction
Insertion compounds
Polarons
Lithium batteries

ABSTRACT

This paper presents a study on the electrical transport properties of lithiated $Cr_{0.11}V_2O_{5.16}$, which can be used as a rechargeable cathodic material in lithium batteries. Dielectric and conductivity spectra of $Li_xCr_{0.11}V_2O_{5.16}$ powders ($x=0$, 0.05, 0.40 and 1.20) were recorded in a broad frequency range of 10–10^{10} Hz at temperature varying between 300 and 400 K. Complex resistivity diagrams have enabled to obtain thermal behaviors of bulk dc-conductivity. Dielectric relaxations were found, attributed to small polarons and (intersite) bipolarons hopping. The transport properties are shown to be consistent with small polaron and bipolaron conduction models. The change from polaronic to bipolaronic conduction has been evidenced with the increase of the lithium content x from 0.40 to 1.20. This work opens up new prospects for a more fundamental understanding of the electronic transport in relation with the electrochemical properties of $Cr_{0.11}V_2O_{5.16}$.

1. Introduction

Vanadium pentoxide is a conducting material with many features that could be used in various applications. Among them is its use as a rechargeable cathodic material in lithium batteries. This compound, which has been extensively studied during the past [1–6], exhibit a layered structure suitable for ionic intercalation reactions. Lithium cations can be thus easily intercalated in V_2O_5 giving rise to $Li_xV_2O_5$ compounds. Li^+ ions are compensated by excess electrons, reducing V^{5+} into V^{4+} and contributing to the electronic conductivity of $Li_xV_2O_5$. Magnetic susceptibility, conductivity, EPR and ENDOR studies [7–12] have confirmed the existence of small-polarons and inter-site bipolarons in these systems. The inter-site small bipolarons [8] are bound states of two neighboring V^{4+} ions stabilized by a large lattice distortion. Previous papers have shown that the electrical conduction of $Li_xV_2O_5$ is only due to small-polarons for low lithium contents ($x<0.50$) [9,10,13]. The cycling of the electrochemical system Li/V_2O_5 presents a good reversibility up to 1 mol of lithium, attributed to the topotactic formation of three phases α, ε and δ. However, a loss of reversibility beyond $x=1$ is observed; this is due to the γ phase which coexists with the δ phase beyond that x value. The insertion of Cr^{3+} ions in the V_2O_5 xerogel permits to obtain the oxide $Cr_{0.11}V_2O_{5.16}$, with a structure similar to that of orthorhombic V_2O_5 (Fig. 1) [14–16]. The formation of (O–Cr–O–Cr–O) short chains linking the V_2O_5 layers enhances electrochemical performances [14–16] when compared to that of V_2O_5. During electrochemical cycling, only both phases α ($x<0.18$) and ε ($x>0.3$) of $Li_xCr_{0.11}V_2O_{5.16}$ are obtained because the (O–Cr–O–Cr–O) chains strengthen the structure and hinder the apparition of the δ and γ phases [14–16]. The performances of a cathodic material are strongly depending upon their electrical properties since electronic species and cations take place during charge–discharge mechanisms. In these systems, the electronic conductivity dominates since the electrons have often the highest mobility. Previous results have shown that $Li_xV_2O_5$ compounds are essentially electronic conductors since their ionic conductivity (from 10^{-7} to 10^{-6} S cm^{-1} at room temperature) is much lower than their electronic conductivity (from 10^{-4} to 10^{-2} S cm^{-1} at room temperature) [12]. In $Li_xCr_{0.11}V_2O_{5.16}$, the lithium diffusion coefficient was previously determined between 10^{-8} and 10^{-11} cm^2 s^{-1} depending on x between 0 and 1.2 [16]. These values being similar to those of $Li_xV_2O_5$, the ionic conductivity of $Li_xCr_{0.11}V_2O_{5.16}$ will be in the range of 10^{-7}– 10^{-6} S cm^{-1} as for $Li_xV_2O_5$ at room temperature.

The study of electrical properties shows some difficulties since the compounds are made in powder form, such as $Li_xCr_{0.11}V_2O_{5.16}$. So, the conductivity measurements by dc and low-frequency techniques cannot give any information on electrical transport properties owing to the existence of microstructures and/or

* Corresponding author.
E-mail address: jc-badot@chimie-paristech.fr (J.C. Badot).

0022-4596/$ - see front matter © 2011 Elsevier Inc. All rights reserved.
doi:10.1016/j.jssc.2011.10.006

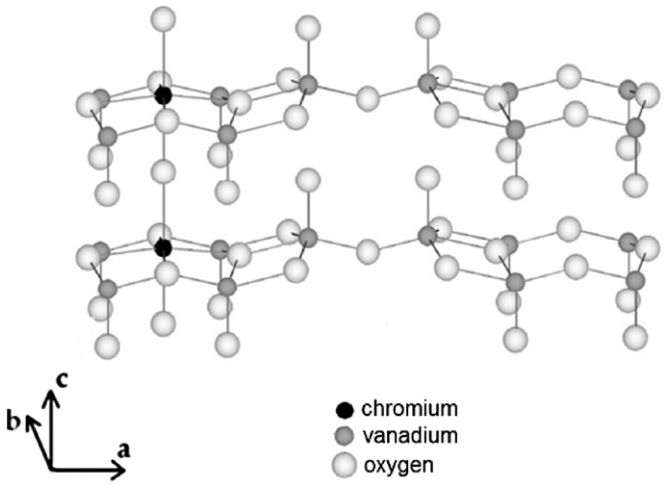

Fig. 1. Schematic structure of $Cr_{0.11}V_2O_{5.16}$ [14–16].

nanostructures. On the other hand, broadband dielectric spectroscopy (BDS) techniques are powerful tools for the electrical characterization of powdered materials [13,17–22]. The BDS probes the interaction of a macroscopic sample with a time-dependent electric field. The resulting polarization, either expressed by the frequency dependent complex permittivity and conductivity, characterizes amplitude and time scale (via the relaxation time) of the charge-density fluctuations within the sample. Such fluctuations arise from the reorientation of the permanent dipole moments, the bound-charge local motions and quasi-blocking grain boundaries in conducting polycrystalline samples. The timescale (or relaxation time) of these fluctuations depends on the relevant relaxation mechanism and the spatial-scale of the sample. In inorganic compounds, these fluctuations generally arise from the reorientation of dipolar species (e.g., water in hydrates) or from the charge local hopping (e.g., ions, protons, polarons and/or bipolarons) at higher frequencies. Odogaki et al. [23] have studied the stochastic transport in one-dimensional hopping conductors (electronic or ionic), in which two or more kinds of hopping rates are distributed regularly. If we consider a double-well system between two finite potential barriers, the Odogaki model [23] predicts one Debye dielectric relaxation. According to Fröhlich [24] and Bosman and van Daal [25], the Debye dielectric relaxation can only occur with small-polaron formation in low-mobility semiconductors [24–26]. Dielectric relaxations due to bipolarons motions were also observed in crystallized compounds such as $SrTiO_3$ and $KTaO_3$ [27]. The dielectric relaxation time corresponds to the hopping time of the charge and is generally thermally activated. Other possible mechanisms include the appearance of interfacial charges fluctuations (e.g. polarization reversal due to the presence of grain boundaries) at lower frequencies. In brief, when the frequency increases, the different kinds of polarization appear in the following order: (a) polarization of the particles (grains) aggregates (low-frequency range); (b) polarization of particles (grains) (low-frequency range); and (c) orientational polarization due to local charge motions (radio- and microwave frequency ranges) [22]. Dielectric spectroscopy has successfully evidenced polaron transport in $Li_xV_2O_5$ [13] and in several glassy vanadate systems [28–30].

In the present paper, we report a detailed study concerning the influence of the lithium insertion on the electronic transport in electroactive vanadium bronzes $Li_xCr_{0.11}V_2O_{5.16}$. The electrical properties were recorded in a broad frequency range of 10–10^{10} Hz within the temperature range of 300–400 K. The study of local motions of charge (polarons and bipolarons) will also be discussed in order to understand the electronic conductivity of $Li_xCr_{0.11}V_2O_{5.16}$ with respect to the temperature.

2. Experimental

2.1. Synthesis

Vanadium pentoxide gels were prepared via the acidification of a sodium metavanadate solution $NaVO_3$ (0.1 M) through a proton exchange resin (DOWEX 50W-X1, 50–100 mesh) [31,32]. A yellow solution of decavanadic acid was initially obtained which polymerizes slowly to a dark red gel. The gel was spread into a thin layer on a glass plate and after drying at room temperature a xerogel with the composition $V_2O_5-1.6H_2O$ was obtained. Intercalation of the Cr^{3+} ions was realized by direct immersion of a V_2O_5 xerogel sample in a 0.1 M solution of $M(NO_3)_3$ [14–16]. After heat treatment at 520 °C during 2 h, a mixed oxide corresponding to the formula $Cr_{0.11}V_2O_{5.16}$ was obtained. $Li_xCr_{0.11}V_2O_{5.16}$ compounds ($x=0$, 0.05, 0.40 and 1.20) were synthesized by reduction of $Cr_{0.11}V_2O_{5.16}$ with n-buthyllithium according to the method described by Whittingham and Dines [33]. The lithium content of lithiated powder samples was controlled by ICP-AES. X-ray powder diffraction study of $Li_xCr_{0.11}V_2O_{5.16}$ was previously performed with Siemens D5000 diffractometer [14–16]. Note that the existence of aggregates constituted by smaller grains (or platelets) has been previously observed by SEM image of the similar compound V_2O_5 synthesized by the same route and heated above 500 °C [17] (Fig. 2).

2.2. Broadband dielectric spectroscopy

Complex resistivity and permittivity spectra were recorded over a broad frequency range of 10–10^{10} Hz, using simultaneously two network analyzers HP 8751 (from 10 to 10^8 Hz) and HP 8510 (from 4.5×10^7 to 10^{10} Hz). The experimental device, fully described in previous papers [13,17–22], consists of a coaxial cell (APC7 standard) in which the cylindrically shaped sample (radius = 1.5 mm and thickness ≈ 1 mm) with silver plated front faces, fills the gap between the inner conductor and a short circuit. After a relevant calibration of the analyzers, the sample admittance Y_s is computed from measurements of the complex reflection coefficient of the device. The knowledge of Y_s allows determining the complex (relative) permittivity $\varepsilon(\omega)=\varepsilon'(\omega)-i\varepsilon''(\omega)$ of the sample. The knowledge of the permittivity enables the calculation of the complex resistivity $\rho(\omega)=[i\omega\varepsilon_0\varepsilon(\omega)]^{-1}$ (ε_0 being the vacuum permittivity) and conductivity $\sigma(\omega)=[\rho(\omega)]^{-1}$ whose real part $\sigma'(\omega)$ will be hereafter called the

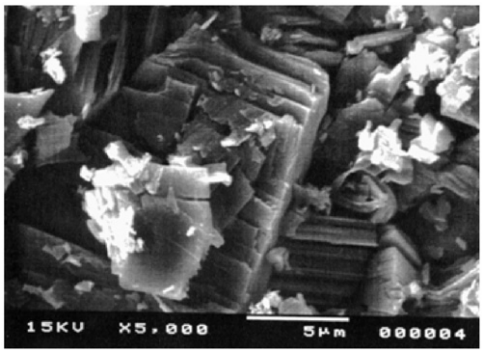

Fig. 2. Scanning electron microscopy image of V_2O_5 obtained by sol–gel process and heated at 500 °C [17].

frequency-dependent conductivity. Complete dielectric spectra were made from about 400 measurement points with an accuracy of approximately 3–5% in the experimental frequency range. The samples are compacted powders at 0.7 GPa and the measurements were made in the temperature range of 300–400 K.

3. Results and discussion

The electric spectra (ε', ε'' and σ' vs. frequency) of the different samples are portrayed in Fig. 3 at 300 K. The real and imaginary parts (ε' and ε'') of the permittivity of $Li_xCr_{0.11}V_2O_{5.16}$ ($x=0.05$, 0.40 and 1.20) are shown in Fig. 3a and b. The frequency-dependent conductivity (real part) $\sigma'=\omega\varepsilon_0\varepsilon''(\omega)$ is also reported in Fig. 3c. For each lithium content, these spectra are nearly similar whatever the temperature. When the frequency increases, the real part of the conductivity increases by 2 to 4 orders of magnitude depending on the lithium content x. On the other hand, the real and imaginary parts of the permittivity decrease strongly in the same frequency range. The imaginary part $\varepsilon''(\omega)$ of the complex permittivity shows a low-frequency dispersion (Fig. 3b), which can be approximated by a straight line with a slope close to −1. Such a behavior corresponds to a to a power-law frequency response ω^{-n} with $n=0.8$–0.9, in the low-frequency domain, i.e. $(\omega/2\pi)<10^4$ Hz for $x=0.05$–0.40 and $(\omega/2\pi)<10^6$ Hz for $x=1.20$. This type of behavior corresponds to a small power-law frequency dependence of the conductivity (real part) $\sigma\propto\omega^s$ with $s=(1-n)=0.1$–0.2 (Fig. 3c). Dc-conductivity regime is hidden owing to polarizations due to resistive and capacitive silver/sample junctions. These phenomena often involve high (real parts) permittivities, i.e. $10^4<\varepsilon'<10^6$ in all the samples (Fig. 3a). For $Li_{0.05}Cr_{0.11}V_2O_{5.16}$ and $Li_{0.40}Cr_{0.11}V_2O_{5.16}$, intense relaxations appear at frequency around 10^5 Hz with maxima of dielectric losses (ε'') of about 10^4 at 300 K. These relaxations are mainly due to interfacial polarizations (aggregate and grain boundaries polarizations) considering their intensity. As the relaxations do not appear clearly in the spectra, the use of Nyquist plots for complex parameters (ρ'' vs. ρ' and ε'' vs. ε') is very helpful. To provide evidence for the relaxations, we used a decomposition procedure of the Nyquist plots for complex resistivity, which has been described elsewhere [13,17–22]. The complex resistivity plots are essentially useful to obtain the grain bulk dc-conductivity in powdered compounds. As an illustration of the decomposition process, Fig. 4a shows the entire complex resistivity diagram, $\rho''=f(\rho')$, of $Li_{0.05}Cr_{0.11}V_2O_{5.16}$ at $T=394$ K. In the mid-frequency part of the plot, the first dispersion domain R1 is well fitted by a circular arc, which corresponds to resistivity relaxation described by the following complex function

$$\rho(\omega)=\rho_H+\frac{\rho_L-\rho_H}{1+(i\omega\tau_\rho)^{1-\alpha}} \quad (1)$$

where ρ_L and ρ_H are, respectively, the low- and high-frequency limits of the resistivity, τ_ρ the (resistivity) relaxation time and α a fitting parameter ($0<\alpha<1$). Note that a small contribution R0 appears at lower frequencies and is due to contact resistance between the silver paint and the sample. After subtracting the contribution of the domain R1, the Nyquist plot of Fig. 4b is obtained. A relaxation R2 is plotted and well fitted by a circular arc with 30 measurement points between 5×10^5 and 5×10^6 Hz. It is thus described by the complex function (1) and crosses the real axis at $\rho'=\rho_m$. Since the aggregates are less conducting than the grains, we may thus assign the relaxation domains R1 and R2 to aggregate and grain boundaries resistances and capacitances, respectively. ρ_m is thus the mean resistivity of the grain bulk. Similar complex resistivity plots are obtained whatever the temperature and for $Li_{0.40}Cr_{0.11}V_2O_{5.16}$. Fig. 4c and d shows that $Li_{1.20}Cr_{0.11}V_2O_{5.16}$ and $Cr_{0.11}V_2O_{5.16}$ are high resistivity compounds: only bulk and R2 relaxations appear. R1 is either shifted towards a lower frequency than the present measurement range, or overlapped with another arc. The grain conductivity $\sigma_m=(\rho_m)^{-1}$ (Fig. 5a) is depending on the temperature and can be ruled by the following expression:

$$\sigma_m=\frac{C}{T}\exp\left(-\frac{W_\sigma}{kT}\right) \quad (2)$$

as in the case of $Li_xV_2O_5$. T is the temperature, k the Boltzmann constant, W_σ the activation energy of the conductivity and C a parameter depending on the kind of the charge carriers (polarons or bipolarons). The room temperature conductivity σ_m and the activation energy W_σ of the different compounds are reported in Table 1. Fig. 5b shows the variation of σ_m with respect to the

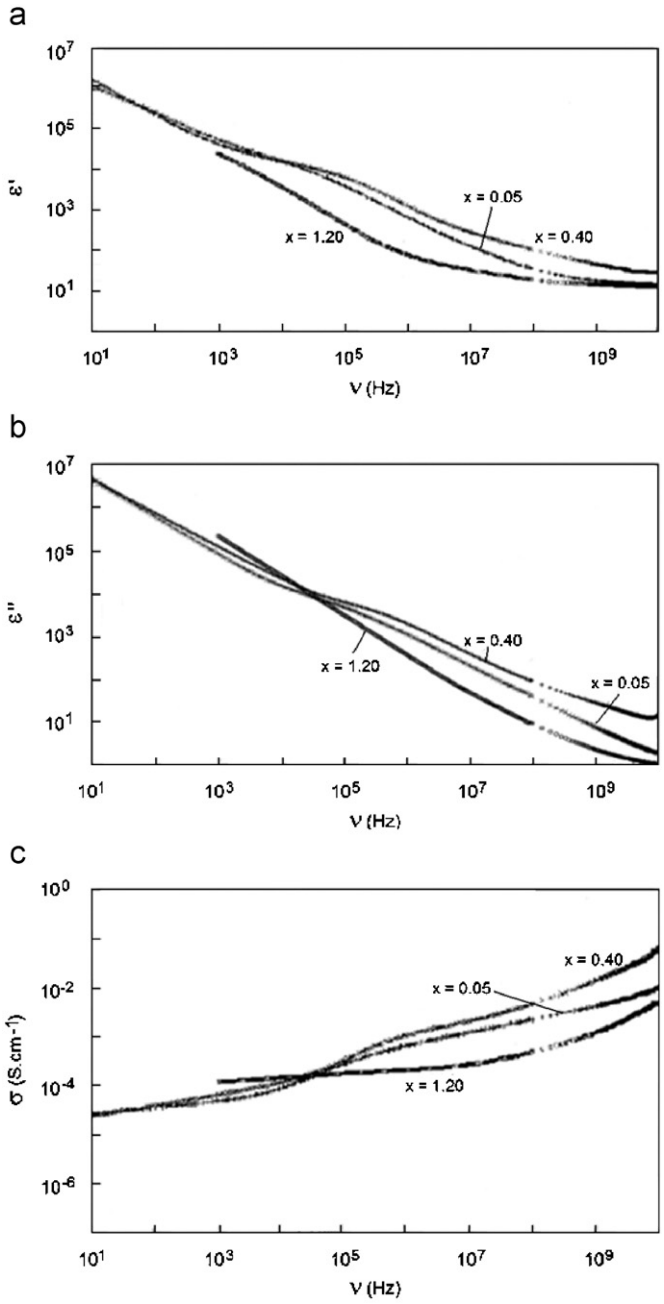

Fig. 3. Electric spectra of $Li_xCr_{0.11}V_2O_5$: (a) real part ε' and (b) imaginary part ε'' of the permittivity vs. frequency $\nu=\omega/2\pi\alpha\tau$ 297 K; and (c) real part of the conductivity σ ($\sigma=\omega\varepsilon_0\varepsilon''$) vs. frequency ν at 297 K.

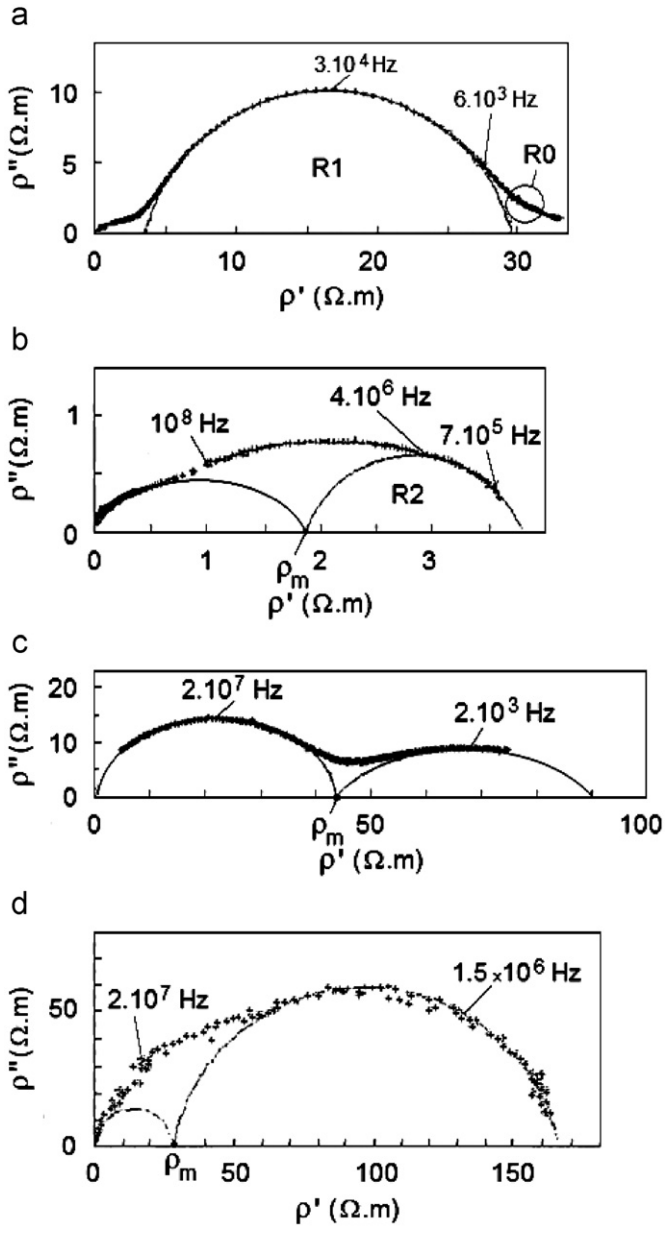

Fig. 4. Nyquist plots of the imaginary part $\rho''(\omega)$ vs. the real part $\rho'(\omega)$ of the complex resistivity for $Li_{0.05}Cr_{0.11}V_2O_5$ (a and b) at 394 K, $Li_{1.20}Cr_{0.11}V_2O_5$ (c) at 300 K and $Cr_{0.11}V_2O_5$ (d) at 373 K. (a) Entire plot from 10 to 10^{10} Hz and evidence of the relaxation R1 (R0 being a small relaxation due to contact resistance and capacitance between silver paint and the sample); (b) plot obtained upon subtracting the domain R1 and evidence of the relaxation domain R2. (c) Entire plot from 10 to 10^{10} Hz: evidence of the bulk relaxation and the relaxation domain R2. (d) Entire plot from 10 to 10^{10} Hz: evidence of the bulk relaxation and the relaxation domain R2. ρ_m represents the resistivity of the grain (crystallite) bulk.

lithium content x ($\log \sigma_m$ vs. x) at room temperature. For the smaller values of x, the rapid rise of σ_m is typical of a percolation transition with a threshold higher than $x \approx 0.05$. It results from the appearance of lithium clusters which form continuous conductive phase (ε phase) above the percolation threshold. A conductivity maximum would occur for lithium content x in the range of 0.20–0.30, as in the case of $Li_xV_2O_5$ in which the ε phase is completely formed. For x between 0.40 and 1.20, the mean conductivity σ_m decreases owing to a probable change of the conduction mechanism, the crystalline symmetry being unchanged.

Otherwise, if the resistivities due to aggregate and grain boundary polarizations are subtracted from the sample resistivity

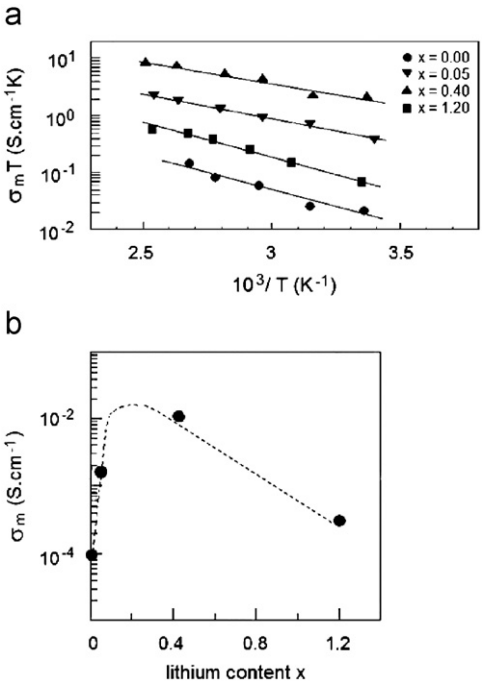

Fig. 5. (a) Grain bulk direct-current conductivity $\sigma_m = \rho_m^{-1}$ as function of inverse temperature T^{-1} (i.e. $\log \sigma_g$ vs. T^{-1}) for $Li_xCr_{0.11}V_2O_5$ (x=0, 0.05, 0.40 and 1.20) at 373 K. (b) Conductivity σ_m as function of lithium content x (i.e. $\log \sigma_g$ vs. x) at 300 K, the dotted line being a guide for the eye.

$\rho(\omega)$, the grain bulk resistivity is given by

$$\rho_m(\omega) = \rho(\omega) - \left[\frac{(\rho_1 - \rho_2)}{1+(i\omega\tau_1)^{1-\alpha_1}} + \frac{(\rho_2 - \rho_m)}{1+(i\omega\tau_2)^{1-\alpha_2}}\right] \quad (3)$$

where τ_1 and τ_2 are the relaxation times of R1 and R2, respectively, $\rho(0)=\rho_1$ and $\rho_m(0)=\rho_m$. The complex permittivity of the grain can thus be expressed by

$$\varepsilon_m(\omega) = \varepsilon'_m(\omega) - i\varepsilon''_m(\omega) = \frac{1}{i\omega\varepsilon_0}\left(\frac{1}{\rho_m(\omega)} - \frac{1}{\rho_m}\right) \quad (4)$$

after subtraction of the dielectric losses due to the grain conductivity. Figs. 6–8 show, respectively, the dielectric spectra (ε_m'' vs. ε_m') for the grains of $Li_{0.05}Cr_{0.11}V_2O_{5.16}$, $Li_{0.40}Cr_{0.11}V_2O_{5.16}$ and $Li_{1.20}Cr_{0.11}V_2O_{5.16}$ at 300 K. To provide evidence for the dielectric relaxations, we used a decomposition procedure of the dielectric spectra, as described in previous papers [13,17–22]. Fig. 6a corresponds to the entire complex permittivity plot of $Li_{0.05}Cr_{0.11}V_2O_{5.16}$. In its low-frequency part, a first dispersion domain P1 is well fitted by a circular arc. P1 corresponds thus to a dielectric relaxation described by the following complex Cole–Cole (CC) function

$$\varepsilon_m = \varepsilon_{mH} + \frac{\varepsilon_{mL} - \varepsilon_{mH}}{1+(i\omega\tau_\varepsilon)^{1-\alpha}} \quad (5)$$

where ε_{mH} and ε_{mL} are the high- and low-frequency limits of the permittivity, τ_n the mean relaxation time and α a fitting parameter ($0<\alpha<1$). The corresponding relaxation frequency $\nu_1=(2\pi\tau_1)^{-1}$ is equal to 6×10^7 Hz at 300 K. After subtracting the contribution of the domain P1, the Cole–Cole plot of Fig. 6b is obtained. A relaxation P2 is plotted and well fitted by a circular arc corresponding to a CC function with a relaxation frequency $\nu_2=10^8$ Hz at 300 K. By the same procedure, a relaxation P3 is unambiguously obtained (Fig. 6c) and described by a CC function with relaxation frequency $\nu_3=1.5\times10^9$ Hz at 300 K. For $Li_{0.40}Cr_{0.11}V_2O_{5.16}$ (Fig. 7), the same relaxations (P2 and P3) are evidenced except the low frequency relaxation P1. Fig. 8 shows that the relaxation

Table 1
Dc-conductivity σ_m of the grains (at 300 K) with its activation energy W_σ. Relaxation frequencies v_1, v_b and v_p (at 300 K) due to the polarization of lithium rich islands, to bipolaron and polaron hopping respectively and their corresponding activation energies W_1, W_p and W_b for different lithium contents x.

Lithium content **x**	Conductivity at 300 K **σ_m (S cm^{-1})** W_σ (eV)	Polarization of lithium rich islands **P1 frequency** v_1 (Hz) W_1 (eV)	Bipolaron hopping **P2 frequency** $v_2=v_b$ (Hz) W_b (eV)	Polaron Hopping **P3 frequency** $v_3=v_p$ (Hz) W_p (eV)	J (meV)[a]	Δ (meV)	ϕ (%)	hv_{ph} (meV)[b]
0.00	10^{-4}	–	–	–	–	–	100	–
	0.24	–	–	–				
0.05	1.5×10^{-3}	6.0×10^{7}	1.0×10^{8}	1.5×10^{9}	6	40	100[c]	36
	0.17	*0.17*	*0.13*	*0.11*				
0.40	8.7×10^{-3}	–	1.0×10^{8}	1.5×10^{9}	6	40	100	36
	0.15	–	*0.13*	*0.11*				
1.20	3.5×10^{-4}	–	3.5×10^{8}	5.5×10^{9}	14	40	0	77
	0.25	–	*0.15*	*0.13*				

[a] $J=8$ meV for V_2O_5
[b] $hv_{ph}=28$ meV for V_2O_5 [7–10].
[c] Most probable value

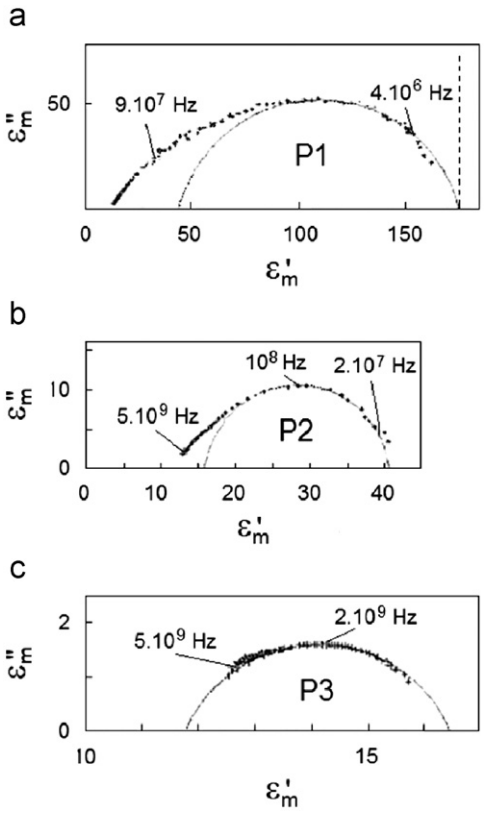

Fig. 6. Cole–Cole plots of the imaginary part $\varepsilon_m''(\omega)$ vs. the real part $\varepsilon_m'(\omega)$ of the complex permittivity for $Li_{0.05}Cr_{0.11}V_2O_5$ at 300 K: the contributions of the grain bulk dc-conductivity σ_m and the interfacial polarizations (grain boundaries and Ag/sample interfaces) have been subtracted. (a) Evidence of the relaxation P1; (b) plot obtained after subtracting the contribution P1 and evidence of relaxation P2; and (c) plot obtained after subtracting the contribution of the relaxation P2 and evidence of relaxation P3.

frequencies of P1, P2 and P3 follow the Arrhenius law given by

$$v_n = v_{n0}\,\exp\left(-\frac{W_n}{kT}\right) \quad (n=1,2 \text{ or } 3) \tag{6}$$

where v_{n0} is the prefactor and W_n the activation energy. The activation energies of the relaxations P2 and P3 are the same for the two compounds $Li_{0.05}Cr_{0.11}V_2O_{5.16}$ and $Li_{0.40}Cr_{0.11}V_2O_{5.16}$ and have respective values $W_2=0.13$ eV and $W_3=0.11$ eV. The activation energy of P1 in $Li_{0.05}Cr_{0.11}V_2O_{5.16}$ is higher, i.e. $W_1=0.17$ eV.

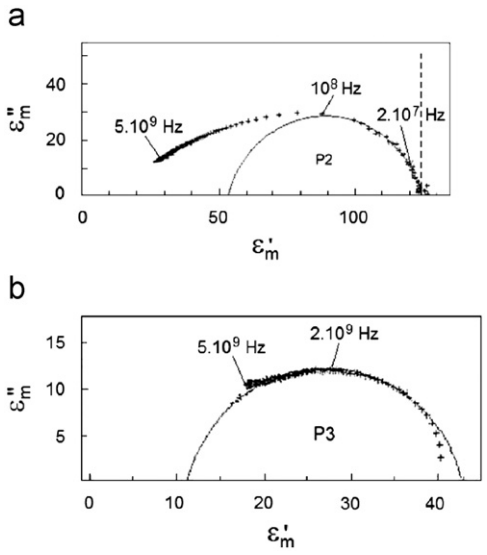

Fig. 7. Cole–Cole plots of the imaginary part $\varepsilon_m''(\omega)$ vs. the real part $\varepsilon_m'(\omega)$ of the complex permittivity for $Li_{0.40}Cr_{0.11}V_2O_5$ at 300 K: the contributions of the grain bulk dc-conductivity σ_m and the interfacial polarizations (grain boundaries and Ag/sample interfaces) have been subtracted. (a) Evidence of the relaxation P2; and (b) plot obtained after subtracting the contributions of the relaxation P2 and evidence of the relaxation P3.

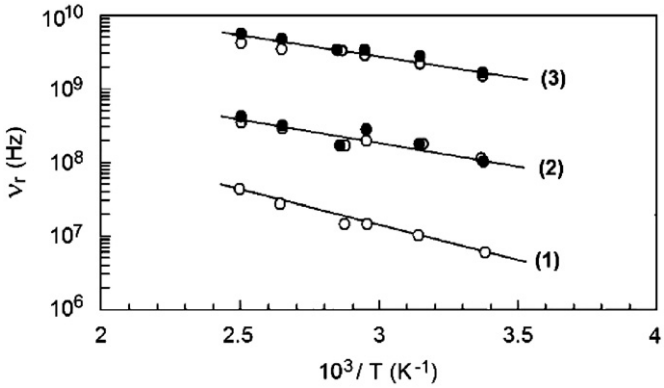

Fig. 8. Relaxation frequencies due to polaron (P3) and bipolaron (P2) hopping as functions of inverse temperature T^{-1} (log v_r vs. T^{-1}) in (a) $Li_{0.05}Cr_{0.11}V_2O_5$ (○) and $Li_{0.40}Cr_{0.11}V_2O_5$ (●); (b) P1 corresponds to the relaxation due to the polarization of the conducting rich lithium islands in $Li_{0.05}Cr_{0.11}V_2O_5$.

For $Li_{1.20}Cr_{0.11}V_2O_{5.16}$ (Fig. 9), only the relaxations P2 and P3 are observed with characteristic frequencies higher but in the same order of magnitude as for the precedent compounds: $v_2 = 3.5 \times 10^8$ Hz and $v_3 = 5.5 \times 10^9$ Hz at 300 K. Their activation energies W_2 and W_3 are slightly higher and equal to 0.13 and 0.15 eV (Fig. 10 and Table 1). As $Li_{0.05}Cr_{0.11}V_2O_{5.16}$ is not a percolated system, we can deduce that the low-frequency relaxation P1 is the consequence of an interfacial polarization between lithium rich islands (high conducting regions) and the $Cr_{0.11}V_2O_{5.16}$ matrix (low conducting region). The relaxations P2 and P3 are thus due to electronic species motions such as small polaron and bipolaron hopping. The hopping regime of these charge-carriers are generally observed in the high-temperature region, i.e. for $T > h\nu_{ph}/2k$ [34]. Furthermore, v_2, v_3, v_{20}, v_{30}, W_2 and W_3 will be hereafter called v_b, v_p, v_{b0}, v_{p0}, W_b and W_p, respectively (b and p indices corresponding to bipolaron and polaron). As W_b is slightly higher than W_p, the theoretical model of Bryksin and Gol'tsev [35,36] allows the attribution of the relaxations P2 and P3 to intersite-bipolaron and small-polaron hopping, respectively. In the bipolaron model proposed by Chakraverty et al. [8], the intersite bipolaron corresponds to the pair V^{4+}–V^{4+} which has a spin singlet ground state $S=0$.

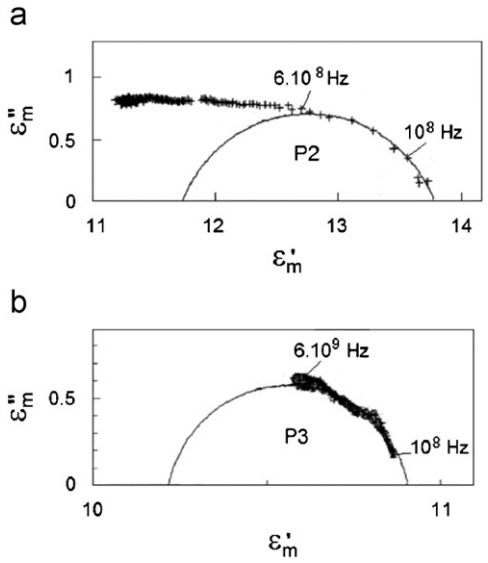

Fig. 9. Cole–Cole plots of the imaginary part $\varepsilon_m''(\omega)$ vs. the real part $\varepsilon_m'(\omega)$ of the complex permittivity for $Li_{1.20}Cr_{0.11}V_2O_5$ at 300 K: the contributions of the grain bulk dc-conductivity σ_m and the interfacial polarizations (grain boundaries and Ag/sample interfaces) have been subtracted to obtain. (a) Evidence of the relaxation P2; and (b) plots obtained after subtracting the contributions of the relaxations P2 and evidence of relaxations P3.

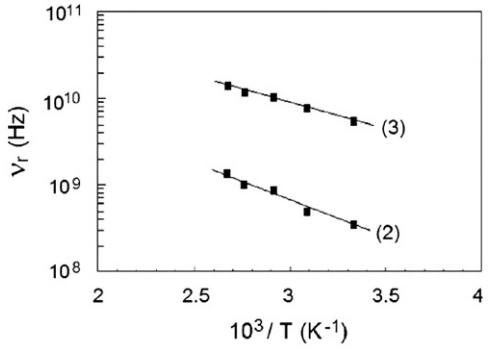

Fig. 10. Relaxation frequencies due to polaron (P3) and bipolaron (P2) hopping as functions of inverse temperature T^{-1} (log v_r vs. T^{-1}) in $Li_{1.20}Cr_{0.11}V_2O_5$ (■).

Considering the prefactors of the relaxation P3, the expression (7) gives $v_{03} \approx 1.5 \times 10^{11}$ Hz for $Li_{0.05}Cr_{0.11}V_2O_{5.16}$ and $Li_{0.40}Cr_{0.11}V_2O_{5.16}$ and $v_{03} \approx 5 \times 10^{11}$ Hz for $Li_{1.20}Cr_{0.11}V_2O_{5.16}$. As the prefactors v_{03} are lower than the phonon frequencies ($v_{ph} \approx 10^{12}$ to 10^{13} Hz), the results seem compatible with non-adiabatic small-polaron hopping. In this later case, the (non-adiabatic) hopping frequency v_p is determined by the following equation [8,35,36]:

$$v_p = \frac{\pi^{1/2} J^2}{2h(W_p kT)^{1/2}} \exp\left(-\frac{W_p}{kT}\right) \tag{7}$$

where h is the Planck constant and J the integral for electron transfer between neighboring sites. The prefactor of Eq. (6) has a very small variation in the present experimental temperature range: (a) $v_{p0} \approx 1.4 \times 10^{11}$ to 1.6×10^{11} Hz for $Li_{0.05}Cr_{0.11}V_2O_{5.16}$ and $Li_{0.40}Cr_{0.11}V_2O_{5.16}$ and (b) $v_{p0} \approx 4.4 \times 10^{11}$ to 5×10^{11} Hz for $Li_{1.20}Cr_{0.11}V_2O_{5.16}$. Fig. 11 shows the temperature dependence of characteristic relaxation frequency (i.e. $\log(v_p.T^{1/2})$ vs. $10^3/T$) corresponding to the (non-adiabatic) small-polaron hopping in $Li_{0.05}Cr_{0.11}V_2O_{5.16}$ (Fig. 11a), $Li_{0.40}Cr_{0.11}V_2O_{5.16}$ (Fig. 11a) and $Li_{1.20}Cr_{0.11}V_2O_{5.16}$ (Fig. 11b). Table 1 summarizes the values of v_p, W_p and J determined from fitting results of Fig. 11 in Eq. (7). The order of magnitude of the transfer integrals J (J=6–14 meV) is the same as that of V_2O_5 (J=8 meV). This result is due to the conservation of the distance V–V of the structural framework despite the presence of lithium and chromium.

It is possible to determine the drift mobility of the bipolarons in the high temperature regime, i.e. for $T > h\nu_{ph}/2k$. In this case, the hopping frequency is written as [35,36]

$$v_b = \frac{16\pi^{3/2} J^4 (kT)^{1/2}}{h(h\nu_{ph})^2 (W_p)^{1/2} (\Delta + 4W_p)} \exp\left[-\frac{(\Delta + 4W_p)^2}{16kTW_p}\right] \tag{8}$$

where Δ is the bipolaron binding (dissociation) energy and v_{ph} the frequency of optical phonons. The intersite bipolaron has an activation energy of the same order as the single polaron activation energy since $\Delta \ll 4W_p$. From this approximation, the hopping

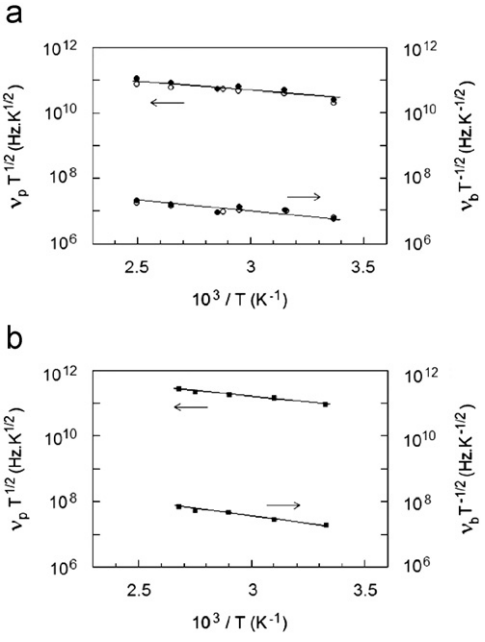

Fig. 11. Hopping frequencies vs. inverse temperature for non-adiabatic polaron (i.e. $\log[v_pT^{1/2}]$ vs. T^{-1}) and bipolaron ($\log[v_bT^{-1/2}]$ vs. T^{-1}) hopping in: (a) $Li_{0.05}Cr_{0.11}V_2O_5$ (○) and $Li_{0.40}Cr_{0.11}V_2O_5$ (●); (b) $Li_{1.20}Cr_{0.11}V_2O_5$ (■).

frequency of an intersite bipolaron will be

$$v_b \approx \frac{4\pi^{3/2}J^4(kT)^{1/2}}{h(hv_{ph})^2(W_p)^{3/2}}\exp\left[-\frac{W_b}{kT}\right] \quad (9)$$

where $W_b \approx W_p + \Delta/2$, W_b being the intersite bipolaron activation energy. The prefactor of Eq. (9) has a very small variation in the present experimental temperature range: (a) $v_{b0} \approx 1.6\times10^{10}$ to 1.8×10^{10} Hz for $Li_{0.05}Cr_{0.11}V_2O_{5.16}$ and $Li_{0.40}Cr_{0.11}V_2O_{5.16}$ and (b) $v_{b0} \approx 8\times10^{10}$ to 9×10^{10} Hz for $Li_{1.20}Cr_{0.11}V_2O_{5.16}$. Fig. 11 shows the temperature dependence of characteristic relaxation frequency (i.e. $\log(v_b.T^{-1/2})$ vs. $10^3/T$) corresponding to the intersite bipolaron hopping in $Li_{0.05}Cr_{0.11}V_2O_{5.16}$ (Fig. 11a), $Li_{0.40}Cr_{0.11}V_2O_{5.16}$ (Fig. 11a) and $Li_{1.20}Cr_{0.11}V_2O_{5.16}$ (Fig. 11b). The values of hv_{ph} obtained from the best fits of Fig. 11 and Eq. (8) are shown in Table 1. These values (hv_{ph}=36–77 meV) seem acceptable as phonon energies and are higher than those of V_2O_5 (hv_{ph}= 28 meV) [7–10], which would be due to the lithium insertion and the presence of (O–Cr–O–Cr–O) short chains linking the V_2O_5 layers.

The electrical conduction of $Li_xCr_{0.11}V_2O_{5.16}$ can be considered as a combination of polaron and bipolaron hopping transfers. In the above models, small polaron and bipolaron conductivities are proportional to their hopping frequencies. The total conductivity σ associated to the polarons (σ_p) and the bipolarons (σ_b) is given by

$$\sigma = \phi\sigma_p + (1-\phi)\sigma_b \quad (10)$$

with

$$\sigma_p = \frac{N_0 f(1-f)(ea)^2}{kT}2\pi v_p \exp\left(-\frac{\delta W_p}{kT}\right) \quad (11)$$

$$\sigma_b = \frac{N_0 f(1-f)(2ea)^2}{2kT}2\pi v_b \exp\left(-\frac{\delta W_b}{kT}\right) \quad (12)$$

where ϕ is the percentage of the conductivity due to the polarons, $\delta W_p=(W_\sigma-W_p)$, $\delta W_b=(W_\sigma-W_b)$ and W_σ the activation energy of the conductivity. The quantities $N_0 \approx 10^{26}$ cm^{-3}, a=0.36 nm and $f=x/2$ are, respectively, the concentration of lattice sites, the hopping distance and the occupation ratio of a vanadium site. For the bipolaron conductivity σ_b, the factor 2 appears because the bipolaron charge is $2e$. Nevertheless, the electronic transfer occurs only along b axis as for V_2O_5 [9]. Since the sample is an isotropic compacted powder, its mean conductivity will be thus $\sigma_m=\sigma/3$. The room temperature conductivity was calculated only for both monophased compounds $Li_{0.40}Cr_{0.11}V_2O_5$ and $Li_{1.20}Cr_{0.11}V_2O_5$. From the experimental data (Table 1) and Eq. (10)–(12), the results are:

(a) $(\sigma_p/3)=8.3\times10^{-3}$ S cm^{-1} and $(\sigma_b/3)=8\times10^{-5}$ S cm^{-1} for $Li_{0.40}Cr_{0.11}V_2O_5$;
(b) $(\sigma_p/3)=4.6\times10^{-3}$ S cm^{-1} and $(\sigma_b/3)=4.2\times10^{-4}$ S cm^{-1} for $Li_{1.20}Cr_{0.11}V_2O_5$.

The comparison of these values with the mean conductivity σ_m gives $\sigma_m \approx \sigma_p/3$ for $Li_{0.40}Cr_{0.11}V_2O_5$ (i.e. $\phi \approx 100\%$) and $\sigma_m \approx \sigma_b/3$ for $Li_{1.20}Cr_{0.11}V_2O_5$ (i.e. $\phi \approx 0\%$). The polaron motions dominate thus the electronic transport in $Li_{0.40}Cr_{0.11}V_2O_5$ (and for $x<0.40$), whereas the bipolaron motions dominate the electronic transport in $Li_{1.20}Cr_{0.11}V_2O_5$. The transition from polaronic to bipolaronic conduction can thus explain the electronic conductivity drop as x increases from 0.40 to 1.20. In this way, the polaron motions became progressively confined within the crystalline framework. Table 1 shows that W_p and W_b are lower than W_σ for $Li_{0.40}Cr_{0.11}V_2O_5$ and $Li_{1.20}Cr_{0.11}V_2O_5$, respectively. The differences $\delta W_p=(W_\sigma-W_p)\approx 0.04$ eV and $\delta W_b=(W_\sigma-W_b)\approx 0.10$ eV are due to Coulomb interactions lithium-polaron and lithium-bipolaron, respectively. Note that lithium-bipolaron interaction is approximately two times higher than that of a single polaron. A similar change from polaronic to bipolaronic conduction was not observed in the lithiated parent oxides $Li_xV_2O_5$ (i.e. for x=0.05 and 0.40) [13]. In α and ε phases of $Li_xV_2O_5$, the bipolarons are not stable because their binding energies Δ=17–25 meV [37] are lower than the experimental thermal energies ($kT>26$ meV). The bipolaron stability in $Li_{0.40}Cr_{0.11}V_2O_5$ is due to higher binding energy Δ=40 meV.

4. Conclusion

In this paper is reported the first determination of the conductivity and the permittivity of $Li_xCr_{0.11}V_2O_5$ compacted powders over a wide frequency range of 10–10^{10} Hz. Complex resistivity and permittivity diagrams have allowed the determination of the electrical transport properties of $Li_xCr_{0.11}V_2O_5$ particles with the temperature from 300 to 400 K. Bulk dc-conductivities were obtained vs. temperature considering the interfacial phenomena. In summary, different dielectric relaxations were shown on $Li_xCr_{0.11}V_2O_5$, resulting from the polarizations at the different scales of the samples: (i) polaron and bipolaron hopping in the crystalline framework, (ii) grains (crystallites) and (iii) aggregates of grains. The change from polaronic to bipolaronic conduction has been evidenced with the increase of the lithium content x from 0.40 to 1.20.

We have shown that the dielectric spectroscopy measurements can provide meaningful information regarding the small-polaron dynamics and the influence of the microstructure on the electronic transport in powdered compounds $Li_xCr_{0.11}V_2O_5$. It is clear that the knowledge of the microstructure is of the highest interest to determine the bulk electrical properties of the materials. Hence, it appears that the only way of determining the electrical properties of granular materials is by using dielectric measurements, in a broad frequency range, from low to microwave frequencies.

This work opens up new prospects for a more fundamental understanding of the electronic transport in $Li_xCr_{0.11}V_2O_5$. In the future, it will be pursued by establishing a correlation of electronic conduction with electrochemical behavior of electrodes constituted of $Cr_{0.11}V_2O_5$.

Acknowledgments

The authors are thankful to Dr. J. P. Pereira-Ramos (GESMAT ICMPE, Thiais, France) for his interest in the work.

References

[1] J. Livage, Chem. Mater. 3 (1991) 578.
[2] M.S. Whittingham, J. Electrochem. Soc. 123 (1976) 315.
[3] J.P. Pereira-Ramos, R. Messina, J. Perrichon, Solid State Ionics 40 (1990) 974.
[4] D. Guyomard, in: T. Osaka, M. Datta (Eds.), New trends in electrochemical technology: energy storage systems for electronics, Gordon & Breach Science Publishers, New York, 2000, p. 253.
[5] C.W. Kwon, A. Vadivel Murugan, G. Campet, J. Portier, B.B. Kale, K. Vijaymohanan, J.H. Choy, Electrochem. Commun. 4 (2002) 384.
[6] C. Delmas, S. Brèthes, M. Ménétrier, J. Power Sources 34 (1991) 113.
[7] V.A. Ioffe, I.B. Patrina, Phys. Status Solidi 40 (1974) 897.
[8] B.K. Chakraverty, M.J. Sienko, J. Bonnerot, Phys. Rev. B 17 (1978) 3781.
[9] C. Sanchez, M. Henry, J.C. Grenet, J. Livage, J. Phys. C: Solid State Phys. 15 (1982) 7133.
[10] C. Sanchez, M. Henry, R. Morineau, M.C. Leroy, Phys. Status Solidi 122 (1984) 175.
[11] M. Bose, A. Basu, J. Solid State Chem. 81 (1989) 30.
[12] B. Pecquenard, D. Gourier, D. Caurant, J. Phys. Chem. 100 (1996) 9152.
[13] B. Pecquenard, J.C. Badot, N. Baffier, N.E. Belhadj-Tahar, Phys. Status Solidi (a) 159 (1997) 469.

[14] P. Soudan, J.P. Pereira-Ramos, J. Farcy, G. Grégoire, N. Baffier, Solid State Ionics 135 (1–4) (2000) 291.
[15] C. Léger, S. Bach, P. Soudan, J.P. Pereira-Ramos, Solid State Ionics 176 (15–16) (2005) 1365.
[16] J.P. Pereira-Ramos, P. Soudan, R. Baddour-Hadjean, S. Bach, Electrochim. Acta 56 (2011) 1381.
[17] F. Ragot, J.C. Badot, N. Baffier, A. Fourrier-Lamer, J. Mater. Chem. 5 (1995) 1155.
[18] J.C. Badot, V. Bianchi, N. Baffier, N.E. Belhadj-Tahar, J. Phys.: Condens. Matter 14 (2002) 6917.
[19] B. Rotenberg, A. Cadène, J.F. Dufrêche, S. Durand-Vidal, J.C. Badot, P. Turq, J. Phys. Chem. B 109 (2005) 15548.
[20] L. Beluze, J.C. Badot, R. Weil, V. Lucas, J. Phys. Chem. B 110 (2006) 7304.
[21] J.C. Badot, L. Beluze, O. Dubrunfaut, J. Phys. Chem. C 112 (2008) 14549.
[22] J.C. Badot, E. Ligneel, O. Dubrunfaut, D. Guyomard, B. Lestriez, Adv. Funct. Mater. 19 (2009) 2749.
[23] T. Odagaki, M. Lax, R.S. Day, Phys. Rev. B 30 (1992) 6911.
[24] H. Fröhlich, Adv. Phys. 3 (1954) 325;
H. Fröhlich, Arch. Sci. 10 (1957) 5.
[25] A.J. Bosman, H.J. van Daal, Adv. Phys. 19 (1970) 1.
[26] G.L. Sewell, Phys. Rev. 129 (1963) 597.
[27] A. Levstik, C. Filipic, V. Bobnar, R. Pirc, Appl. Phys. Lett. 81 (2002) 4046.
[28] S. Mandal, A. Gosh, J. Phys.: Condens. Matter 8 (1996) 829.
[29] S. Sen, A. Gosh, Phys. Rev. B 60 (1999) 15143.
[30] S. Bhattacharya, A. Gosh, Phys. Rev. B 68 (2003) 224202.
[31] P. Aldebert, N. Baffier, N. Gharbi, J. Livage, Mater. Res. Bull. 16 (1981) 669.
[32] J.J. Legendre, J. Livage, J. Colloid Interface Sci. 94 (1983) 75.
[33] M.S. Whittingham, M.B. Dines, J. Electrochem. Soc. 124 (9) (1977) 1387.
[34] T. Holstein, Ann. Phys. 8 (1959) 343.
[35] V.V. Bryksin, A.V. Gol'tsev, Sov. Phys. Solid State 30 (5) (1988) 851.
[36] A.S. Alexandrov, N.F. Mott, Polarons and Bipolarons, World Scientific, Singapore, 1995.
[37] B. Pecquenard, Thesis, Paris, 1995.